SUPPLEMENTAL MATERIALS

Rapid rebalancing of excitation and inhibition by cortical circuitry

Alexandra K. Moore, Aldis P. Weible, Timothy S. Balmer, Laurence O. Trussell, and Michael Wehr

Figure S1

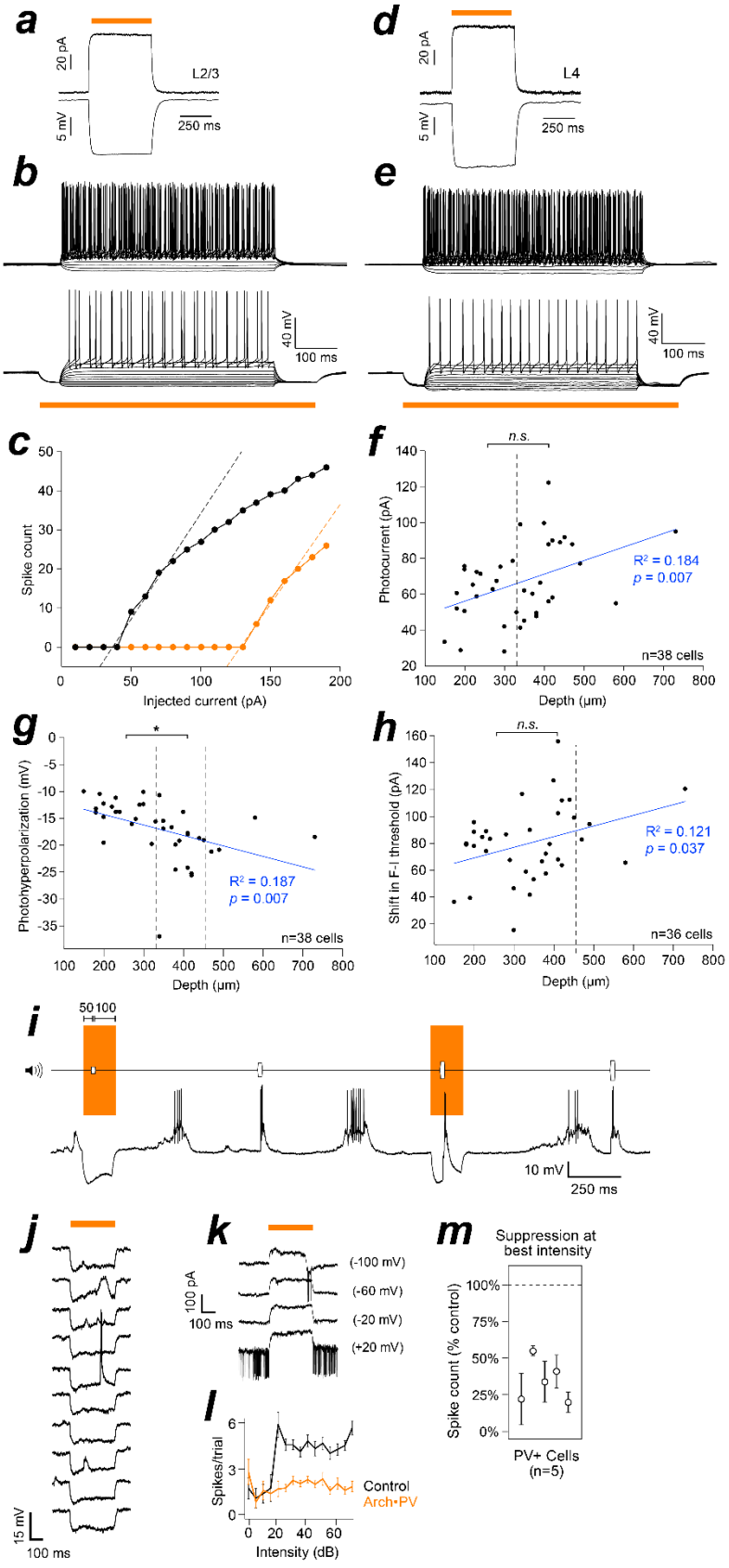
a
20 pA
5 mV
L2/3
250 ms
d
20 pA
5 mV
L4
250 ms
b
40 mV
100 ms
e
40 mV
100 ms
c
Spike count
Injected current (pA)
f
n.s.
Photocurrent (pA)
R² = 0.184
p = 0.007
n=38 cells
Depth (µm)
g
*
Photohyperpolarization (mV)
R² = 0.187
p = 0.007
n=38 cells
Depth (µm)
h
n.s.
Shift in F-I threshold (pA)
R² = 0.121
p = 0.037
n=36 cells
Depth (µm)
i
50 100
10 mV
250 ms
j
15 mV
100 ms
k
100 pA
100 ms
(-100 mV)
(-60 mV)
(-20 mV)
(+20 mV)
l
Spikes/trial
Intensity (dB)
Control
Arch•PV
m
Suppression at best intensity
Spike count (% control)
PV+ Cells (n=5)

Figure S1 (related to Figures 1 & 4) – Intracellular measurements of Arch currents in PV+ neurons

In vitro measurements of Arch photocurrents and photohyperpolarization

We targeted whole-cell recordings to Arch-GFP+/PV+ cells in auditory cortex slices to measure the strength of Arch photocurrents and photohyperpolarization. PV+ cells in all layers showed robust and reliable responses to laser illumination. **a-c**, Example recording from a L2/3 PV+ cell showing the response to a 500 ms laser pulse (**a**) and 20 pA current steps with and without illumination (**b**). We quantified the shift in spike threshold (**c**) by fitting a line to the first 5 current steps that evoked spikes and then measuring the shift in x-intercept. **d-e**, Example recording from a L4 PV+ cell, same format as panels a-b.

f-h, Group data. Dashed lines indicate laminar boundaries between L2/3, L4, and L5 (Anderson et al., 2009); linear regression is shown in blue. The strength of suppression increased slightly but significantly with recording depth. **f**, Steady-state photocurrent measured in 38 PV+ cells. There was no significant difference in photocurrent between L2/3 and L4 neurons (rank-sum, p=0.19, n=18 L2/3 cells and 16 L4 cells). **g**, Steady-state photohyperpolarization measured in 38 PV+ cells. Photohyperpolarization was significantly greater in L4 PV+ cells than in L2/3 PV+ cells (rank-sum, p=0.0004). **h**, Shift in F-I thresholds in 36 PV+ cells, measured as in panel c. There was no significant difference in threshold shift between L2/3 and L4 neurons (rank-sum, p=0.29).

Suppression of spiking responses in vivo

We used the blind patch technique to confirm that Arch produced hyperpolarizing photocurrents and suppressed sound-evoked spiking in PV+ neurons *in vivo*. Arch-expressing cells were unambiguously identified by their reliable responses to green light (n=7 PV+ neurons, depths 296-406 μm; note that these cells were all located in L4). **i-k**, Example recording from a L4 PV+ cell. **i**, Voltage response to 25 ms white noise (WN) bursts with laser pulses on alternating trials (orange shading). **j**, Membrane potential response to 10 consecutive laser pulses (pulse duration, 400 ms). **k**, Outward Arch currents measured at different holding potentials in voltage-clamp mode. Each trace shows a single trial. Light-evoked currents were highly reliable and did not reverse, regardless of holding potential, consistent with the action of a proton pump.

We recorded spiking responses in a subset of cells (5/7 L4 PV+ cells without channel blockers in the internal solution) and compared the response to sounds presented alone ("control" trials) and sounds embedded in a laser pulse ("Arch•PV" trials). **l**, Mean spiking response to white noise (WN) bursts at different intensities for an example PV+ cell. Stimuli: WN from 0-70 dB, in 5 dB steps; 20 stimulus repetitions in each condition. Error bars show SEM. Spiking was suppressed across a range of sound levels in each case (Skillings-Mack, $p<0.05$ for 5/5 PV+ cells). **m**, Spiking responses on Arch•PV trials as a percentage of the control response, n=5 PV+ cells. Points show the median change across best stimuli for each cell; error bars show the interquartile range (IQR). "Best stimuli" were the stimuli that evoked spiking responses in the 75th percentile on control trials, i.e. the most effective 1/4th of the stimulus array for each neuron.

Figure S2

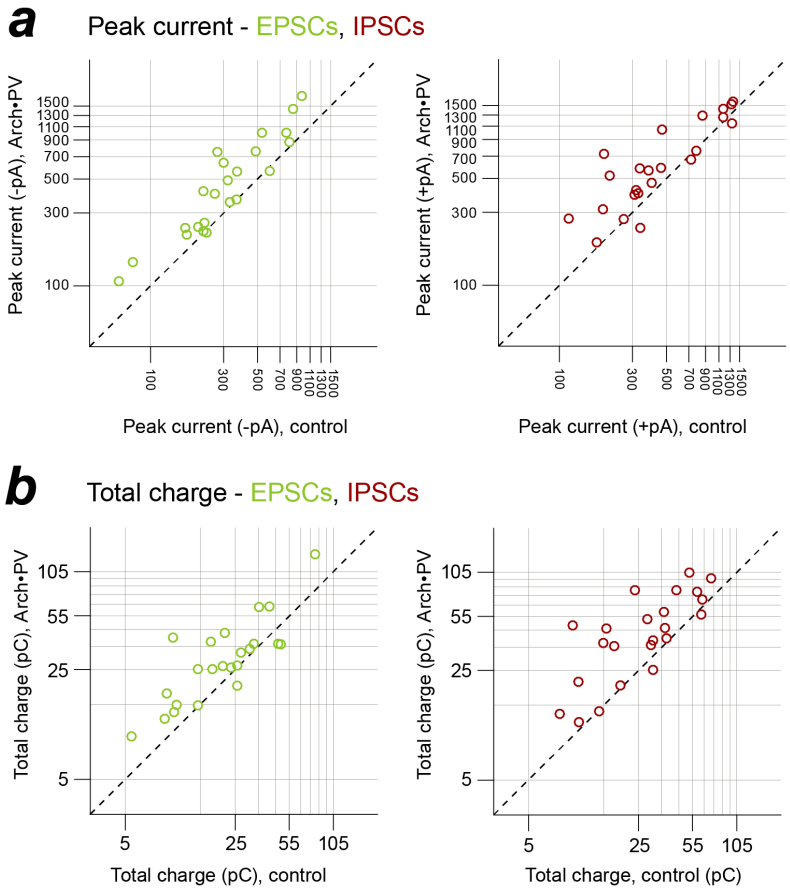

Figure S2 (related to Figures 2 & 3) – Synaptic currents in PNs

Voltage clamp data from Figure 2f, replotted to show absolute changes in peak current and total charge (n=23 PNs). **a**, Peak current amplitude in raw units (pA) for excitatory (left) and inhibitory currents (right). **b**, Same as a, but for total synaptic charge (pC). Values are the trial-averaged response to a single "best stimulus" as in Figure 2f. We did not encounter any PNs that showed a significant reduction in inhibition on Arch•PV trials. Of the 23 PNs in our sample, 15/23 showed a significant increase in IPSCs and 8/23 showed no significant difference between the Arch•PV and control conditions. In the CFF model (Figure 6a-d) Arch stimulation reduces inhibition to PNs in the first layer of the feedforward network, which corresponds to thalamorecipient L4. Our PN sample in L4 was too small (n=2; possibly due to an electrode bias toward larger soma) to provide evidence for or against the possibility that individual PNs in this layer experience a net decrease in inhibition on Arch•PV trials.

Figure S3

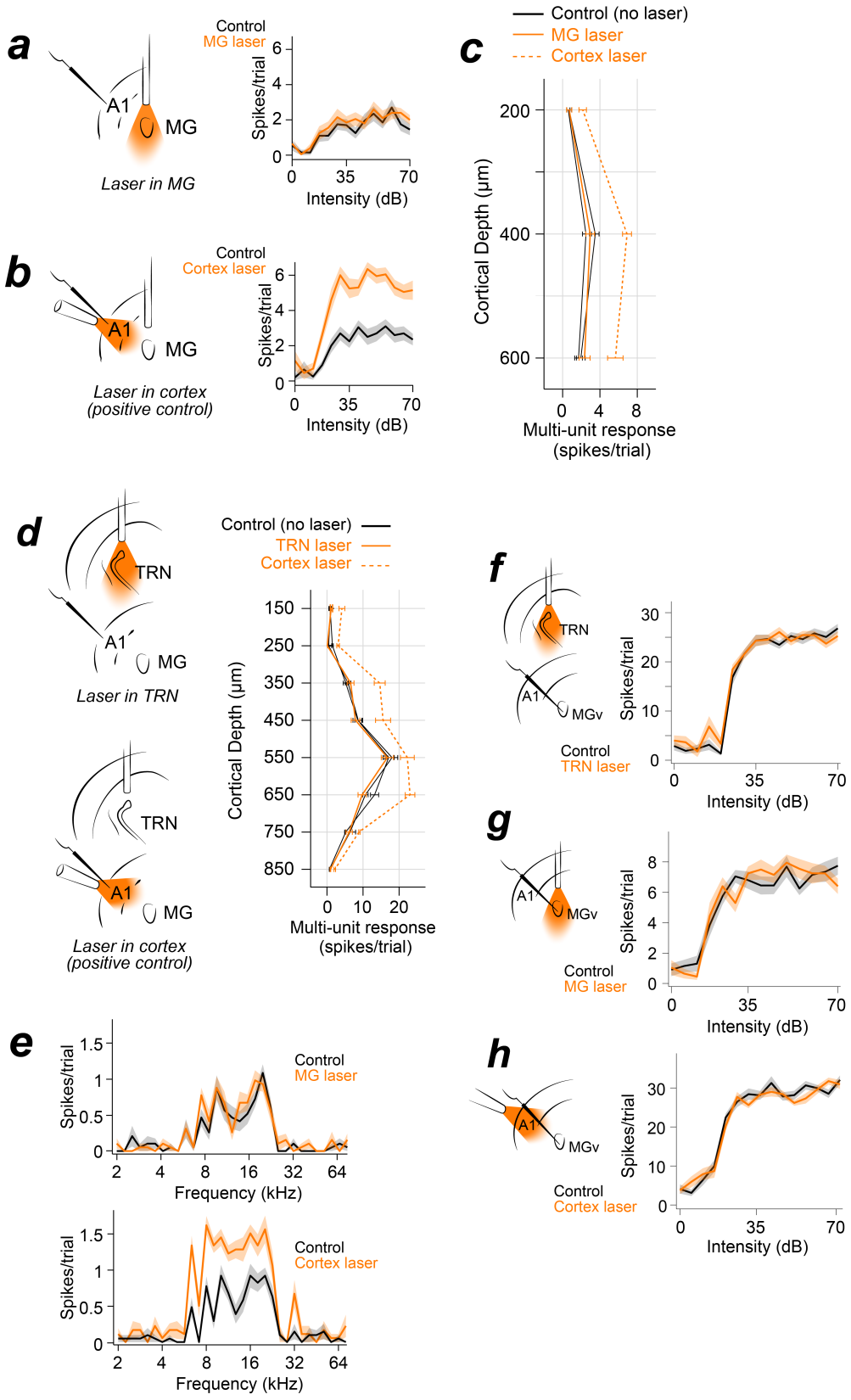
a
A1
MG
Laser in MG
Control
MG laser
Spikes/trial
Intensity (dB)
b
A1
MG
Laser in cortex
(positive control)
Control
Cortex laser
Spikes/trial
Intensity (dB)
c
Control (no laser)
MG laser
Cortex laser
Cortical Depth (µm)
Multi-unit response
(spikes/trial)
d
TRN
A1
MG
Laser in TRN
Laser in cortex
(positive control)
Control (no laser)
TRN laser
Cortex laser
Cortical Depth (µm)
Multi-unit response
(spikes/trial)
e
Control
MG laser
Control
Cortex laser
Spikes/trial
Frequency (kHz)
f
TRN
A1
MGv
Control
TRN laser
Spikes/trial
Intensity (dB)
g
A1
MGv
Control
MG laser
Spikes/trial
Intensity (dB)
h
A1
MGv
Control
Cortex laser
Spikes/trial
Intensity (dB)

Figure S3 (related to Figure 3) – Spiking responses in auditory thalamus are unaffected by laser stimulation, and thus are not responsible for observed changes in cortical activity

We performed several control experiments to rule out the possibility of thalamic involvement in the effects we observed in cortical neurons in transgenic Arch/PV-Cre mice. Our primary concern was that some of the changes we observed could be explained by an increase in feedforward input to auditory cortex on laser trials. How could this occur? The majority of feedforward input to auditory cortex originates from the medial geniculate body of the thalamus (MG), which receives axonal projections from PV-Cre+ inhibitory neurons in the thalamic reticular nucleus (TRN) (Ahrens et al., 2015; Cruikshank et al., 2001; Halassa et al., 2014; Pinault, 2004). In principle, these PV-Cre+ projections could be suppressed by stray light from the cortical surface and have a disinhibitory effect on corticothalamic relay neurons in MG. We tested this possibility in the following experiments.

Laser pulses delivered directly to thalamic nuclei have no effect on activity in A1

We recorded spiking activity in auditory cortex while illuminating the MG through an implanted fiber to see if we could reproduce the effects of light delivered from the cortical surface. **a-b**, Multi-unit spiking responses at an example recording site in A1. Light was delivered to the MG through an implanted fiber (a), or a fiber positioned at the cortical surface (b). Light pulses delivered from the cortical surface produced an increase in spiking, whereas pulses delivered to the MG had no effect. Stimuli: WN bursts from 0-70 dB; responses are the mean±SEM over 20 stimulus repetitions. **c**, Multi-unit responses to WN at an intermediate intensity of 50 dB at different recording depths in the same animal. Solid orange line: light delivered to the cortical surface; dashed orange line: light delivered to the MG. We repeated this experiment at multiple depths across the tonotopic gradient of A1 in 4 mice (n=21 recording sites in total). 18/21 sites showed an increase in spiking in response to cortical illumination, whereas 0/21 sites showed a change in responsiveness with MG illumination (Skillings-Mack, $p>0.05$). **d**, Same experiment as in a-c, but with a fiber implanted over the TRN instead of the MG (n=13 recording sites in 2 mice). 11/13 sites showed an increase in spiking in response to cortical illumination, whereas 0/13 sites showed a change in response to TRN illumination (Skillings-Mack, $p>0.05$). Consistent with the lack of a change in spike counts, we observed no changes in frequency tuning in response to thalamic illumination. **e**, Cell-attached recording from a cortical PN with a fiber implanted in the MG. Stimului: 2-80 kHz tones at 70 dB. We tested for changes in frequency-intensity tuning in 9 multi-unit and 10 single-unit recordings in 5 mice; 0/19 recordings showed a change in tuning in response to MG or TRN illumination (Skillings-Mack, $p>0.05$).

Laser pulses have no effect on spiking responses in auditory thalamus

We recorded MG responses in the same animals to further verify that there was no change in subcortical activity on laser trials. **f-h**, Multi-unit responses recorded in the ventral division of MG (MGv), with illumination of the TRN (f), MG (g), and cortical surface (h). 0/12 sites showed a change in activity when light was delivered to these three locations (Skillings-Mack, $p>0.05$).

Together, these experiments rule out the possibility that the effects we observed in cortex were due to changes in subcortical activity. The following observations provide further evidence that the effects we observed were the result of suppressing PV+ activity within auditory cortex. First, it is highly unlikely that the light power used in the main experiments would be sufficient to reach the

MG, which is located >2 mm from the cortical surface. Light would be even less likely to reach the TRN, which is located further away on the AP axis. Second, we found that PV+ responses were suppressed in L4 and enhanced in L2/3, whereas we would expect to see the opposite pattern if the increase in PV+ activity were driven by an increase in feedforward input (Cruikshank et al., 2007). Finally, TRN neurons would need to be actively suppressing sound-evoked responses in MG for light to have a disinhibitory effect on thalamocortical projection neurons, but this is probably not the case in our experiments. The TRN receives multi-modal excitatory inputs from sensory cortices and thalamic nuclei (Pinault, 2004) and is thought to be involved in gating or redirecting attention during goal-directed tasks (Ahrens et al., 2015; Halassa et al., 2014). If TRN projection neurons are not engaged by sensory stimuli in the anesthetized or passively awake animal, then TRN suppression would have a negligible effect on MG responses.

Supplemental methods for Figure S3

Fiber placement – Prior to performing a craniotomy over auditory cortex, we implanted an optical fiber dorsal to the MG (n=4 Arch-GFP/PV-Cre mice; AP: -3.1 mm from bregma, ML: 1.8 mm lateral of the midline, DV: 2.3 mm vertical from the cortical surface). The fiber (diameter 0.2 mm) was implanted through a small hole in the skull and fixed in position with grip cement, with the anesthetized animal in a stereotaxic apparatus. Fiber placement was confirmed post-mortem. The same procedure was used to implant fibers over the TRN, except that the fiber was positioned dorsal to (i.e. directly above) the TRN (n=2 mice; AP: -1.3 mm from bregma, ML: 2.0 mm lateral of the midline, DV: 2.3 mm vertical from the cortical surface).

Multi-unit recordings – We recorded multiunit activity using 1-5 MΩ tungsten electrodes, amplified with an AM Systems 1800 extracellular amplifier (band-pass 0.3-5 kHz). Spike times were extracted using a fixed voltage threshold exceeding 5 SD of the baseline extracellular voltage. Spiking responses were analyzed in the 0-100 ms period following the onset of the sound. Auditory cortex was mapped at the beginning of each experiment. After obtaining recordings in A1, we used this map to locate the central region of MGv, which is located approximately 2.3-2.5 mm below the pial surface. We discriminated MGv from other divisions based on its low spontaneous activity, short onset latencies, and relative width along the AP axis (Anderson and Linden, 2011; Hackett et al., 2011).

Figure S4

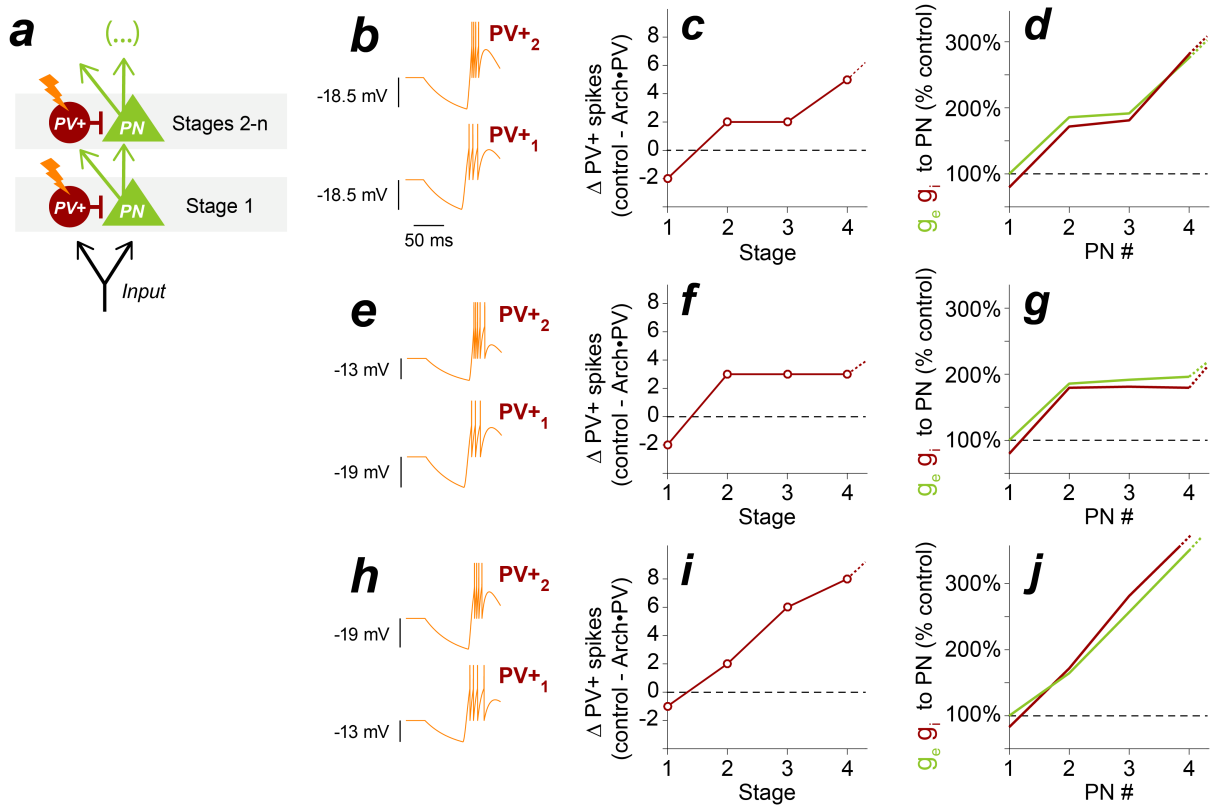

Figure S4 (related to Figure 4) – Excitatory-inhibitory rebalancing is robust to variations in Arch efficacy in a feed-forward circuit model

Our *in vitro* measurements of Arch currents in transgenic mice (Figure S1) showed that PV+ cells in thalamorecipient L4 were slightly more suppressed by full-field illumination than PV+ cells located in L2/3. To confirm that the effects we observed were not simply due to laminar difference in Arch expression, we varied the amount of suppression applied to the PV+ cells in the first and second stages of the circuit model in Figure 4g, which correspond to cortical L4 and L2/3, respectively. **a**, Model schematic. **b-d**, Original model parameters for purpose of comparison. **b**, In the original version of the model, the strength of the suppressive current I_{Arch} is the same in each layer, producing -18.5 mV of hyperpolarization in all PV+ cells. **c**, PV+ spiking is suppressed in the first layer of the circuit, but increases in subsequent layers. **d**, Inhibitory input to the first PN is reduced on Arch trials, whereas PNs in subsequent layers show a coordinated increase in excitation and inhibition. **e-g**, Same format as panels b-d. We adjusted the strength of the Arch current in layers 1 and 2 to produce the average hyperpolarization measured in L4 and L2/3 PV+ cells (L4 cells: -18.9±3.8 mV, L2/3 cells: -13.5±1.4 mV; see Figure S1). The ~5 mV difference in the strength of suppression did not affect the overall behavior of the model: PV+ spiking was suppressed in the first stage of the model, but increased above baseline in subsequent stages. Inhibitory input to the first PN was reduced, resulting in an increase in both excitation and inhibition to PNs in subsequent stages. **h-j**, To test the generality of the rebalancing effect, we then reversed the relative strength of I_{Arch} in the two layers, so that the current applied to the PV+ cell in the first layer of the model matched our

measurements in L2/3 and vice versa. We observed rebalancing here as well. The increase in excitation and inhibition to the second PN was even stronger in this case, in agreement with our modeling results in Figure 6 – stronger suppression produces more rebalancing, not less. Taken together, these results suggest that the effects we observed *in vivo* (the suppression of PV+ responses in L4, versus the enhancement of PV+ responses in L2/3) cannot be explained by a difference in Arch expression between layers.

Figure S5

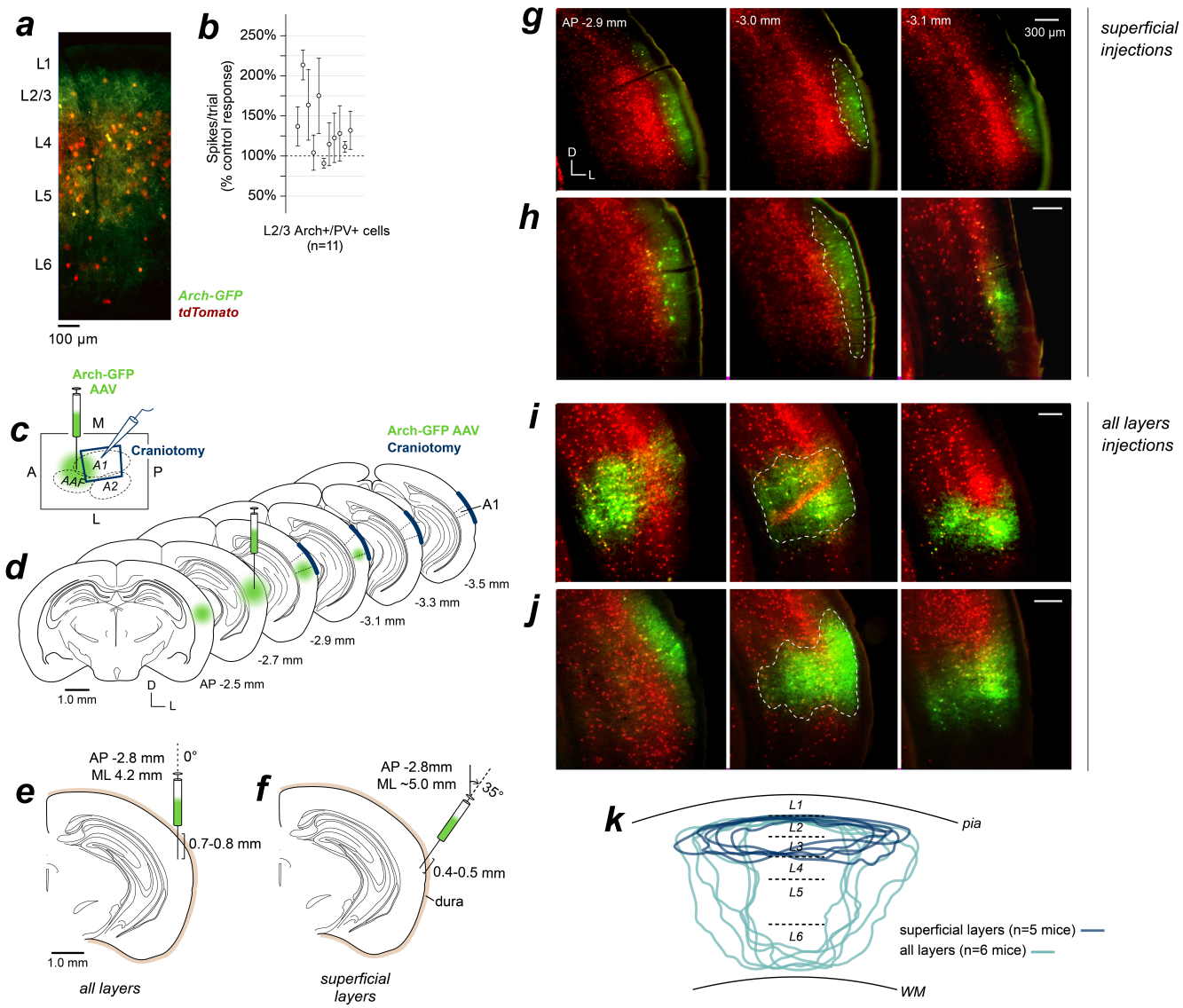

Figure S5 (related to Figures 4 & 5) – Viral expression of Arch-GFP

Viral expression of Arch-GFP in all layers

When Arch expression was limited to L2/3, Arch-positive PV+ neurons were effectively suppressed on laser trials (Figure 5). However. when Arch was expressed in all layers in transgenic Arch-GFP/PV-Cre mice, Arch-positive PV+ neurons showed a net increase in responsiveness on laser trials (Figure 4). To confirm that this difference was related to the spatial extent of Arch expression and not the method of expression itself (viral versus transgenic), we used the viral method to express Arch in PV+ cells in all layers (n=6 mice). In these animals, illumination produced a net increase in L2/3 PV+ activity, as it did in transgenic mice. **a**, Coronal section from a PV-Cre/tdTomato mouse expressing Arch-GFP in layers 1-6 (see STAR Methods). Section thickness,

75 μm. **b**, Spiking responses of Arch-expressing PV+ neurons recorded in L2/3 (n=11 cells, depths 186-271 μm) of all-layer virus injected mice. Points show the median spiking response on Arch•PV trials as a percentage of the control response (median across best stimuli, 50th percentile). Across cells, spiking increased to 128±23% of the control response (median±IQR, n=11 Arch+/PV+ cells), corresponding to a raw change of +1 to +2 spikes/trial for responses to a single intensity, with effect sizes d=0.27-0.56 (IQR). These Arch+/PV+ cells were fast-spiking neurons, with narrow extracellular spike waveforms and high spontaneous firing rates (spike width, 0.89±0.08 ms; spontaneous firing rate 3.7±3.9 Hz; n=11 cells). Note that suppressing PV+ activity in all layers produced a net increase in spiking in Arch-positive PV+ cells in L2/3, but when PV+ activity was suppressed in L2/3 only, these same Arch-positive PV+ cells were effectively suppressed. This suggests that the increase in excitation from disinhibited L2/3 PNs alone was not strong enough to overcome Arch-mediated hyperpolarization in local PV+ cells. From this we conclude that translaminar excitation from L4 PNs made a major contribution to the effects seen in transgenic animals, consistent with the observation that translaminar excitation to PV+ cells is stronger than reciprocal excitation from neighboring PNs in the same layer (Atallah et al., 2012; Hofer et al., 2011).

Methods for viral injections

c-d, Illustration of the viral expression method. Panel c is the view from the cortical surface, panel d shows a series of coronal sections. We targeted viral injections to the anterior region of auditory cortex and opened craniotomies just posterior to the injection site. This approach ensured (1) that the recording site jn A1 was not damaged by injection or local inflammation, and (2) that we were able to target recordings to both Arch-positive and Arch-negative cells in L2/3 for the experiments shown in Figure 5. **e-f**, We used two approaches for viral injection, yielding distinct patterns of infection. We injected the virus at the same location on the AP axis for the "all-layer" and "superficial layer" experiments, but the needle entered the cortex at different angles. To target Arch-GFP expression to PV+ neurons in all layers of auditory cortex, the needle was passed through a 1 mm^2 cranial window (AP: -2.8 mm, ML: 4.2 mm), 0° from the vertical axis, to a depth of 0.7-0.8 mm from the dura. To restrict expression to PV+ neurons in the superficial layers of auditory cortex (L1-3), the needle was passed through a 1mm^2 window immediately ventral to the parietal ridge over auditory cortex (AP: -2.8mm, ML: ~5.0 mm), 35° from the vertical axis, to a depth of 0.4-0.5 mm. **g-j**, Sections from 4 animals. The first two mice (g,h) are superficial-only examples, the second two mice (i,j) are all-layer examples. Sections are 100 μm thick, through the posterior half of the expression site, starting with the most anterior section nearest to the injection site. The fluorescent stripe in i (center image) is a slicing artifact. **k**, Boundary outlines. Each outline corresponds to one section from one mouse (see dashed lines in g-j). We obtained these outlines by aligning the tdTomato images to each other (rigid transformation), then applying the same transformations to the GFP images. We smoothed the aligned GFP images with a gaussian filter, and then determined the outline from the 50th percentile of pixel intensities. Laminar boundaries are from (Anderson et al., 2009); coronal atlas images are adapted from (Paxinos, 2013).

Figure S6

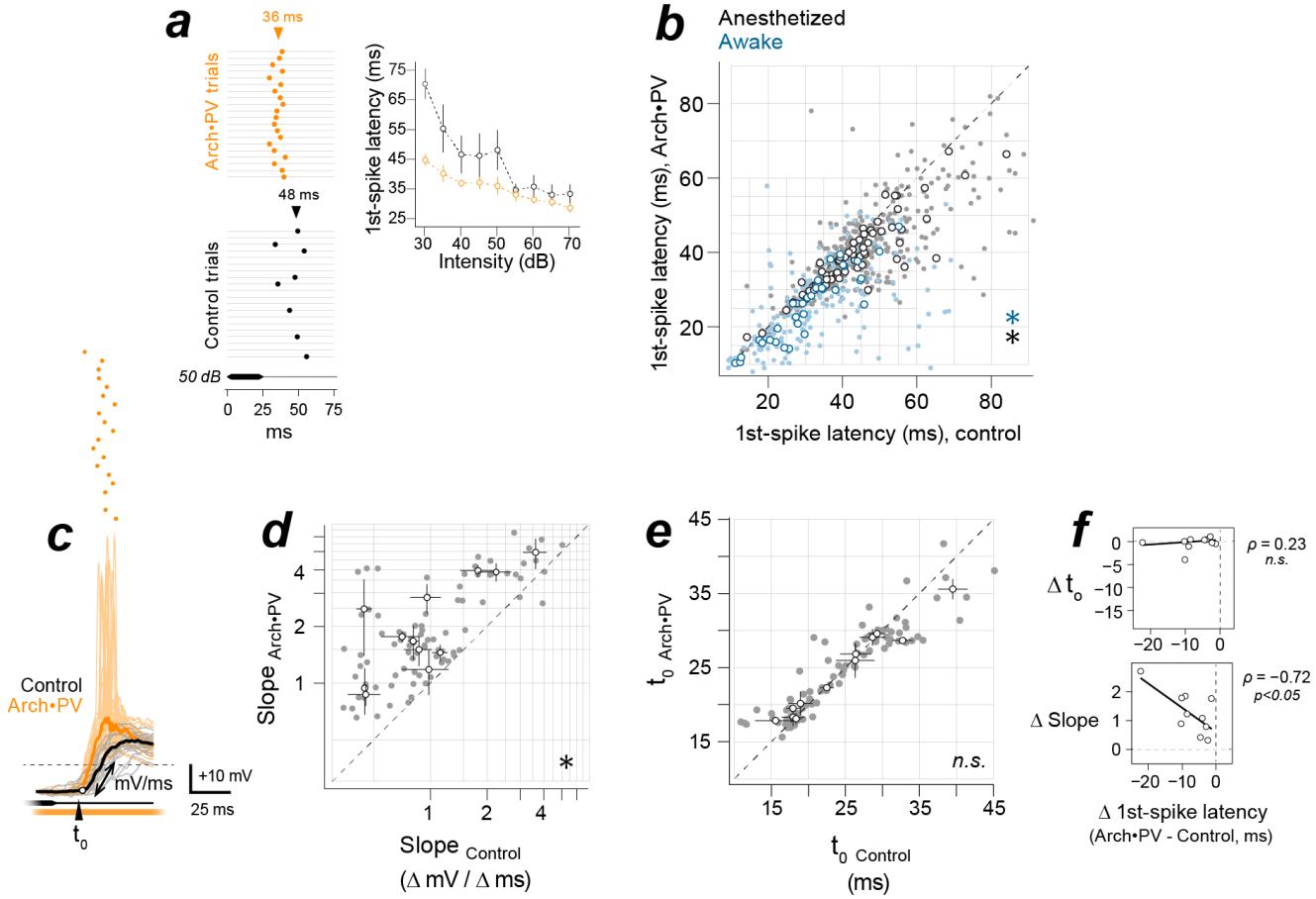

Figure S6 (related to Figure 7) – PN spike latency decreases on Arch•PV trials

Illumination had a dramatic effect on the timing of PN spikes. **a**, *Left*: Raster plot showing the spiking response of an example PN to 20 repetitions of a 16 kHz tone (best frequency) at 50 dB. The median spike latency (arrowheads) decreased by 12.5 ms on Arch•PV trials. *Right*: Spike latency values (median±IQR across repetitions) over a range of intensities. Note that the largest changes occur at lower sound intensities. **b**, Summary plot showing the decrease in 1st-spike latency for PNs recorded in anesthetized mice (black symbols, n=65 PNs) and awake mice (blue symbols, n=33 PNs). The change in spike latency was significant for the majority of neurons (anesthetized: 48/65 PNs, awake: 19/33 PNs; Skillings-Mack, $p<0.05$). For cells recorded in anesthetized animals, 1st-spike latency decreased by 4.9 ms (median difference) from 43.0±7.1 ms on control trials to 38.1±6.1 ms on Arch•PV trials (signed-rank, $p<0.05$, $d=0.43$, n=65 cells). Cells recorded in awake mice had shorter latencies in general, but showed a similar change on Arch•PV trials: 1st-spike latency decreased by 4.1 ms, from a median of 30.5±7.8 ms on control trials to 26.4±8.1 ms on Arch•PV trials (signed-rank, $p<0.05$, $d=0.51$, n=33 cells). Open circles show the median across best intensities (1 point per neuron); filled circles show the latencies for single intensities.

To understand the mechanism underlying the decrease in spike latency, we examined the onset and timecourse of sound-evoked potentials in PNs (n=12 recordings without channel blockers in the internal solution). **c**, Membrane potential response to WN at 50 dB. Grey traces: control trials, orange traces: Arch•PV trials; bold lines show the mean for each condition. We measured the slope of the response from the inflection point at t_0 (response onset) to +10 mV above baseline (see Methods for details). **d-e**, Summary of changes in slope (d) and t_0 (e) for n=12 PNs. There was a significant increase in slope (signed-rank, $p<0.001$, $d=0.58$, n=12 PNs) but no difference in onset time on Arch•PV trials (signed-rank, $p=0.52$, $d=0.03$, n=12 PNs). Open circles: median±IQR across best intensities; filled circles: values for individual intensities. **f**, Changes in spike latency versus changes in slope (bottom) and onset time (top) for n=10 PNs (2/12 cells did not spike on control trials). The increase in slope was correlated with the decrease in spike latency (Spearman's $\rho=-0.72$, $p<0.05$, n=10 PNs), but the difference in onset time was not (Spearman's $\rho=0.23$, $p=0.52$, n=10 PNs). Thus, we concluded that the 4-5 ms difference in spike latency was primarily due to an increase in the speed of the postsynaptic membrane potential response, rather than a change in the timing of excitatory input. This is consistent with our PN voltage-clamp recordings, which showed a substantial increase in the size of sound-evoked EPSCs, but little change in timing.

Figure S7

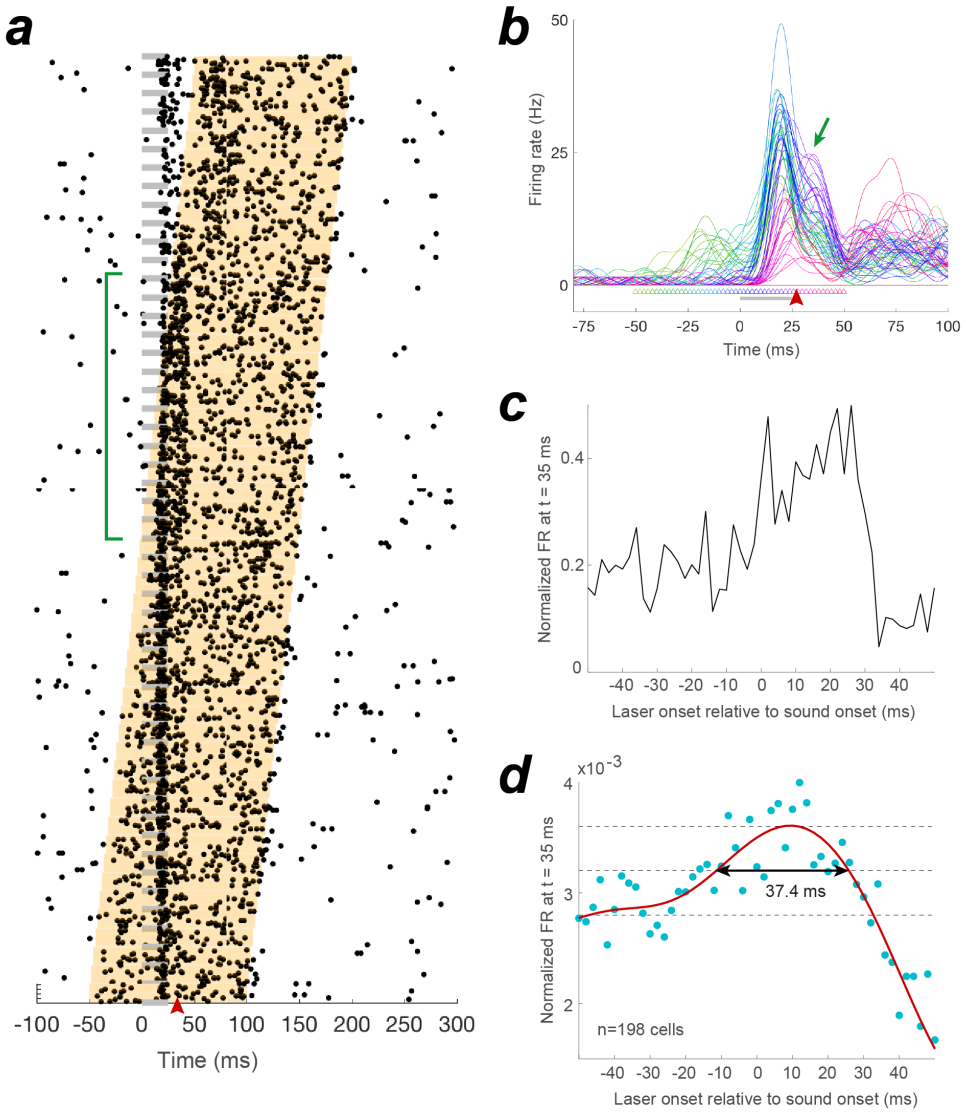

Figure S7 (related to Figure 7) – Relative timing of laser onset and sound onset

To determine how long it takes for rebalancing to manifest at the level of PN spikes, we recorded responses in awake animals with chronically implanted tetrodes while varying the relative timing of laser onset and sound onset. **a**, Responses of an example cell to a white noise burst (25 ms, 60 dB) embedded in a 150 ms laser pulse. We varied the onset time of the laser pulse from -50 ms before sound onset to +50 ms after sound onset (50 repetitions each). Laser timing is indicated by the orange shading. When laser onset occurred less than ~30 ms after sound onset, the duration of the spiking response was prolonged (green bracket). When laser onset preceded sound onset, the trial-to-trial reliability of the spiking response increased with negligible change in response duration, as shown in Figure 7. **b**, Firing rate across all laser onsets for the example cell in panel a. The sound is indicated by horizontal grey bar. Traces are color-coded for laser onset time (-50 to 50 ms relative to sound onset, corresponding to the arrowheads underneath the traces). Firing rate was smoothed by convolution with a 10 ms Gaussian. Note the increase in response duration in

the purple traces (green arrow). **c**, Same cell shown in panels a-b. To quantify the difference in response duration we measured the mean firing rate in a 20 ms window in the latter half of the response period, beginning 35 ms after sound onset (arrowheads in panels a-b). Values are normalized to the maximum firing rate for the cell across all timing conditions. **d**, Group data for n=198 neurons. Blue dots show the population mean for each laser timing condition. Although not all cells showed an increase in response duration, the effect was evident at the population level. Spiking activity in the late response window was greatest when the laser pulse began -10 ms to +30 ms after sound onset, with a half-max width of 37.4 ms. Dashed lines show the baseline and maximum values used to determine the half-max value. When laser onset and sound onset were separated by longer delays (>37 ms), neurons showed an increase in trial-to-trial reliability with no increase in response duration. This indicates that inhibitory rebalancing takes effect within ~40 ms of laser onset.

Figure S8

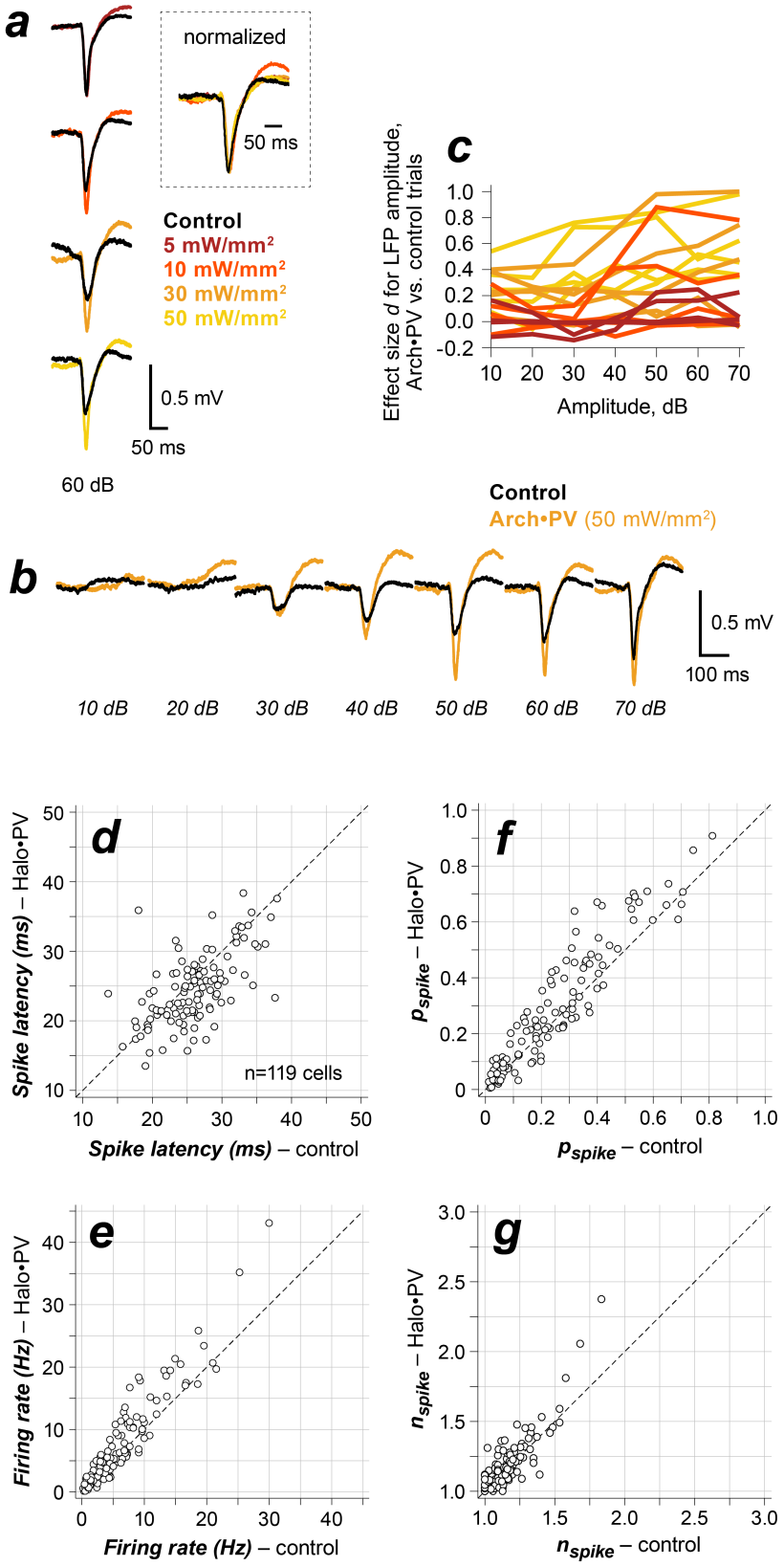
a
normalized
50 ms
Control
5 mW/mm²
10 mW/mm²
30 mW/mm²
50 mW/mm²
0.5 mV
50 ms
60 dB
c
Effect size d for LFP amplitude, Arch•PV vs. control trials
1.0
0.8
0.6
0.4
0.2
0.0
-0.2
10 20 30 40 50 60 70
Amplitude, dB
Control
Arch•PV (50 mW/mm²)
b
0.5 mV
100 ms
10 dB
20 dB
30 dB
40 dB
50 dB
60 dB
70 dB
d
Spike latency (ms) – Halo•PV
Spike latency (ms) – control
n=119 cells
f
p_spike – Halo•PV
p_spike – control
e
Firing rate (Hz) – Halo•PV
Firing rate (Hz) – control
g
n_spike – Halo•PV
n_spike – control

Figure S8 (related to Figures 1-6) – The cortical response to PV+ suppression does not depend on laser power or choice of inhibitory opsin

PV+ suppression with increasing laser power

We verified that laser illumination had a similar effect on sound-evoked activity across a range of light powers in Arch/PV-Cre mice, both above and below the values used in the main experiments (approximately 30±5 mW total power from the fiber tip). We compared local field potential (LFP) responses to laser-interleaved stimuli at 5, 10, 30 and 50 mW/mm^2 power within recording sites (n=5 locations in 3 transgenic mice, recording depths 344±93 μm). **a**, *Left*: LFP responses to 60 dB WN with increasing laser power for an example recording site. Each trace is the mean of 30 stimulus repetitions (control, black traces; Arch•PV, colored traces). The amplitude of the response increased with laser power, but the duration and overall shape of the response did not change. *Right:* Same data, normalized to show that the time course of the response was unaffected. **b**, Responses to WN across a range of sound intensities at 50 mW/mm^2 laser power. Sound-evoked responses were with the normal physiological range, even at maximal laser power. The effect of illumination resembled natural changes in the strength of sensory input. **c**, Group data showing the relationship between laser power and effect size (*d*) for changes in LFP amplitude. Lines show the effect size across intensities at a single laser power (color-coded as in panel a) at n=5 recording sites. Stimuli: 25 ms WN at intensities 0-70 dB, >10 stimulus repetitions in the control and laser conditions at each laser power. Note that the effect size varied smoothly from a large effect at high power down to no effect as laser power approached 0 mW. At no point did the effect change sign.

PV+ suppression with halorhodopsin

To verify that the effects we have described were not specifically linked to our choice of suppressive opsin, we replicated our results using halorhodopsin, a light-activated chloride pump. We expressed the AAV-DIO-halorhodopsin virus in all layers of auditory cortex in 6 PV-Cre mice and recorded the activity of 321 presumed PNs using chronically-implanted tetrodes. Of these neurons, n=119 cells responded to sounds on control trials; non-responsive neurons were excluded from further analysis. Halo activation produced a decrease in spike latency (**d**, signed-rank, p=0.00033, n=191 PNs) and an increase in sound-evoked firing rates (**e**, signed rank, p=0.00002, n=119 PNs). As in Arch/PV+ mice, the increase in firing rate was driven by an increase in trial-to-trial reliability (**f**, p_{spike}) rather than an increase in the number of spikes fired on individual trials (**g**, n_{spike}). Accordingly, PNs showed a significant increase in p_{spike} but no change in n_{spike} at best intensity on laser trials (maximum p_{spike}, p=0.00001, maximum n_{spike} p=0.9124; signed-rank, n=119 PNs). These experiments show that the response to PV+ suppression in Halo/PV-Cre mice is indistinguishable from the response to PV+ suppression in Arch/PV-Cre mice (see Figure 7 & Table S1). Because halorhodopsin is a chloride pump, rather than a proton pump, these results cannot be attributed to any pH-specific effects of archaerhodopsin (Mahn et al. 2016). Consistent with this finding, Kato et al. (2017) recently reported that hyperpolarization of PV+ cells in auditory cortex with Halorhodopsin produces a paradoxical increase of spontaneous synaptic inhibition and excitation in PNs.

Table S1

		Group median±IQR		Signed-rank test
		Control trials	Arch•PV trials	
p_{spike} at best intensity	Anesth. recordings, n=65 PNs	0.80±0.22	0.95±0.10	p<0.0001, d=0.38
	Awake recordings, n=33 PNs	0.75±0.16	0.85±0.08	p<0.0001, d=0.36
n_{spike} at best intensity	Anesth. recordings, n=65 PNs	2.0±0.5 spikes	2.0±0.5 spikes	n.s. p=0.54, d=0.02
	Awake recordings, n=33 PNs	3.0±1.0 spikes	3.0±1.0 spikes	n.s. p=0.82, d=0.02

Table S1 (related to Figure 7) – Group data for changes in PN spiking activity

Group data corresponding to Figure 7d-e. PN spiking responses increased substantially on Arch•PV trials in both awake and anesthetized mice. This was primarily due to an increase in the trial-to-trial reliability of sound-evoked spikes (p_{spike}) rather than an increase in the number of spikes fired on individual stimulus trials (n_{spike}).